

Article

Enhancing the Thermal Stability of Glutathione Bifunctional Synthase by B-Factor Strategy and Un/Folding Free Energy Calculation

Wenlong Zhu, Heming Sun, Qixuan Jiang, Ruonan Zheng, Qingyun Wang, Qinfei Zhang, Luo Liu ^{*}  and Hui Cao ^{*}

Beijing Bioprocess Key Laboratory, Beijing University of Chemical Technology, Beijing 100029, China

^{*} Correspondence: liuluo@mail.buct.edu.cn (L.L.); caohui@mail.buct.edu.cn (H.C.); Tel.: +86-10-64421335 (L.L. & H.C.);

Fax: +86-10-64416428 (L.L. & H.C.)

Abstract: Glutathione is of great significance in pharmaceutical and health fields, and one-step synthesis of reduced glutathione by glutathione bifunctional synthase has become a focus of research. The stability of glutathione bifunctional synthase is generally poor and urgently needs to be modified. The B-factor strategy and un/folding free energy calculation were both applied to enhance the thermal stability of glutathione bifunctional synthase from *Streptococcus agalactiae* (GshFSA). Based on the concept of B-factor strategy, we calculated the B-factor by molecular dynamics simulation to find flexible residues, performed point saturation mutations and high-throughput screening. At the same time, we also calculated the un/folding free energy of GshFSA and performed the point mutations. The optimal mutant from the B-factor strategy was R270S, which had a 2.62-fold increase in half-life period compared to the wild type, and the Q406M was the optimal mutant from the un/folding free energy calculation, with a 3.02-fold increase in half-life period. Both of them have provided a mechanistic explanation.



Citation: Zhu, W.; Sun, H.; Jiang, Q.; Zheng, R.; Wang, Q.; Zhang, Q.; Liu, L.; Cao, H. Enhancing the Thermal Stability of Glutathione Bifunctional Synthase by B-Factor Strategy and Un/Folding Free Energy Calculation. *Catalysts* **2022**, *12*, 1649. <https://doi.org/10.3390/catal12121649>

Academic Editor: C. Heath Turner

Received: 20 November 2022

Accepted: 13 December 2022

Published: 15 December 2022

Publisher's Note: MDPI stays neutral with regard to jurisdictional claims in published maps and institutional affiliations.



Copyright: © 2022 by the authors. Licensee MDPI, Basel, Switzerland. This article is an open access article distributed under the terms and conditions of the Creative Commons Attribution (CC BY) license (<https://creativecommons.org/licenses/by/4.0/>).

Keywords: molecular dynamics simulation; B-factor strategy; thermal stability; glutathione bifunctional synthase

1. Introduction

Reduced glutathione is a tripeptide group composed of glutamic acid, cysteine and glycine, and it is most abundant biothiol in cells. Due to its antioxidant properties, it is widely used in the pharmaceutical, cosmetic and food industries [1].

The traditional method of glutathione biosynthesis was composed of the fermentation method and two-step enzymatic method. The fermentation method was performed by yeast fermentation, which had advantages of easy availability of raw materials and mature process, but this method also had problems such as low yield and difficult separation [2]. The traditional enzymatic method involved γ -glutamylcysteine synthetase (γ -GCS) and glutathione synthetase (GS). The use of GS enzyme was the rate-limiting step of the reaction, which had problems such as low synthesis efficiency [3].

Recently, glutathione bifunctional synthases have been found to perform one-step glutathione production, such as GshF from *Streptococcus sanguinis* (GshFSS) [4], GshF from *Streptococcus thermophiles* (GshFST) [5] and GshF from *Streptococcus agalactiae* (GshFSA) [6]. The reaction requires only three amino acids and ATP to be completed. These glutathione bifunctional synthases all have enzyme activity of about 2 U/mg and highly similar sequences, but all suffer from low thermal stability, which poses a great challenge for the next step of industrial application.

In recent years, attention has been focused on the modification of the thermal stability of biocatalysts. Natural enzyme catalysts are of poor stability, which affects the catalytic efficacy of an enzyme, affects the reusability of an enzyme, and increases the cost of preserving and transporting an enzyme [7].

The following factors are generally considered to affect the thermal stability of proteins: salt bridges, hydrogen bonds, hydrophobic interactions, disulfide bonds, electrostatic interactions, etc. [8]. The hydrophobic interactions were considered to be the most important factor [9]. Protein stability is further divided into thermodynamic and kinetic stability. Thermodynamic stability can be defined as the Gibbs free energy difference between the natural and unfolded conformations of a protein, while the Gibbs free energy difference ΔG_u , melting temperature T_m , and unfolding equilibrium constant K_u are generally used to describe protein thermodynamic stability [10]; protein dynamic stability refers to the resistance to inactivation at a certain temperature. Generally, the half-life $t_{1/2}$ (the time required for enzyme activity to drop to half of its initial level) and T_{50} (the temperature required for enzyme activity to be reduced by half) are used to characterize the dynamic stability of an enzyme [11].

Nowadays, strategies that are widely used to enhance protein stability include directed evolution, evolutionary analysis, un/folding free energy calculations, B-factor, machine learning, artificial design of disulfide bonds, proline strategies, etc. [12,13].

Anthony P. Green et al. used directed evolution to enhance the plastic degradation enzyme PETases and obtained a high thermal stability mutant HotPETase by high-throughput screening, with only a 6% decrease in activity after 24 h incubation at 75 °C [14]. Yang et al. reported that an un/folding free energy calculation could be used to enhance the thermal stability of alginate lyase. They calculated the B-factor and $\Delta\Delta G$ of the enzyme and rationally designed point mutants, and the best mutant H176D had almost twice the half-life period of WT at 50 °C [15]. Machine learning can also be used to guide the modification of enzyme thermal stability. For example, Arnold's group used mutant data obtained from directed evolution as a training set and they used it to guide further modification of P450. The model predicted that the recommended mutant improved the T_{50} value by 8.7 °C [16].

In this study, we used molecular dynamics simulations, based on the protein model constructed by Alphafold2 [17], to predict potential saturation mutation sites under the guidance of B-factor, and performed high-throughput screening. Meanwhile, the un/folding free energy ($\Delta\Delta G$) was also calculated, the sites for point mutations were predicted under the guidance of $\Delta\Delta G$, and the stability was evaluated. Both strategies allowed us to make a rapid global search for dominant mutants and reduce the workload compared to random mutations, which is an excellent method for improving enzyme thermal stability.

2. Results

2.1. Model Construction and MD of GshFSA

Based on the amino acid sequence of GshFSA, we performed the protein model construction and evaluation by Alphafold2. In Alphafold2, it is generally considered that the structure can be used as a reference when scoring over 90, and the model score came to 94.5. We further evaluated the model by SAVES v6.0 (<https://saves.mbi.ucla.edu/>, accessed on 11 November 2021), and the model passed ERRAT, Verify3D, and PROCHECK scoring and testing [18]. The results of ERRAT and Verify 3D were as follows. In ERRAT, the model of GshFSA using Alphafold2 scored 97.15, and passed the test. In Verify 3D, 93.21% of the residues averaged 3D–1D score ≥ 0.2 and passed the test. In Figure 1, the results of PROCHECK showed that residues in the most favored regions came to 92.6%, and residues in the additional allowed regions came to 7.0%. Alphafold2 could build a more realistic protein model for the next step of molecular dynamics simulation.

The protein structure was simulated using Gromacs for 298 K, 318 K and 338 K with 100 ns. After energy minimization, pressure pre-equilibration, and temperature pre-equilibration, root mean square deviation (RMSD) and root mean square fluctuation (RMSF) values were calculated. RMSD is used to indicate the structural changes of the protein simulation process, and RMSF indicates the degree of flexibility of amino acid residues. When describing a protein, the higher the B-factor value, the more unstable and flexible the conformation of that residue is. In molecular dynamics simulation, $RMSF^2 = B \times 3/8/\pi^2$ [19], and so we calculated the B-factor for each residue. According to Figure 2, we found

that the B-factor values of residues in the 117–121 region, 162–166 region, 202–205 region, 267–272 region, and 509–554 region were higher compared to other regions and fluctuated more with increasing temperature. Therefore, residues in this region were preferentially selected as the point saturation mutation sites.

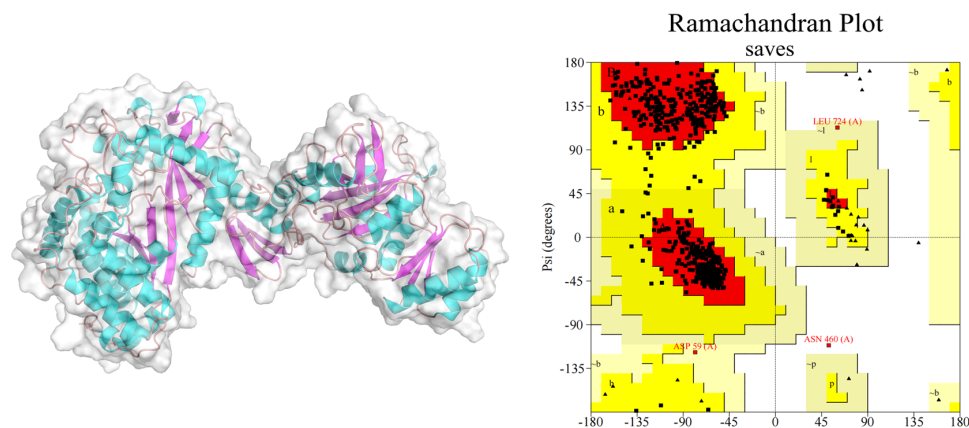


Figure 1. The Structure and Ramachandran Plot of GshFSA.

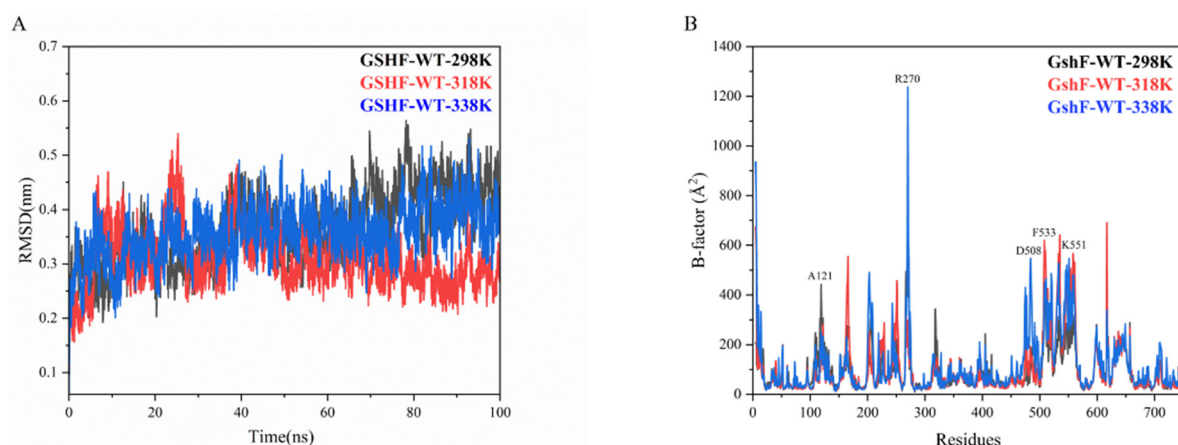


Figure 2. The RMSD and B-factor values of GshFSA. (A) The RMSD values of GshFSA-298 K, GshFSA-318 K and GshFSA-338 K; (B) The B-factor values of GshFSA-298 K, GshFSA-318 K and GshFSA-338 K.

Finally, A121, R270, D508, F533, and K551 were selected as the sites for point saturation mutations, and point saturation mutation libraries were constructed according to the method shown in Section 3.2.

2.2. Screening Results of Point-Saturated Mutant Libraries

According to the method shown in Section 3.4, we constructed the mutant library and completed the high-throughput primary screening of 1600 samples successfully, and a total of 32 positive samples were screened out. These 32 positive samples were re-screened by shake flask and the following results were obtained.

As shown in Figure 3, the mutants were all samples with higher residual enzyme activity than the wild type after heat treatment at 45 °C for 4 min, and there were 17 samples in total. After heat treatment, the residual enzyme activity of the wild type was only 11.4%, which indicated that the GshFSA had low thermal stability and was difficult to use widely as an industrial enzyme. The best mutant was R270S, and the residual enzyme activity was 39.94% of the initial enzyme activity after heat treatment under the same conditions. The site that screened for the most dominant mutants was 121 residue, with five. Here, we only did single-point saturation mutations instead of double-point or multi-point saturation mutations, because the probability of being able to superimpose advantageous mutations

at the same time is not high enough for multi-point simultaneous mutations. Additionally, there is a high probability of an antagonistic effect, which increases the uncertainty. After measuring the half-life of the optimal mutant R270S at 40 °C, its $t_{1/2}$ increased from 5.69 min to 14.88 min compared with the wild type, which was shown in Table 1. This constituted a 2.62-fold increase.

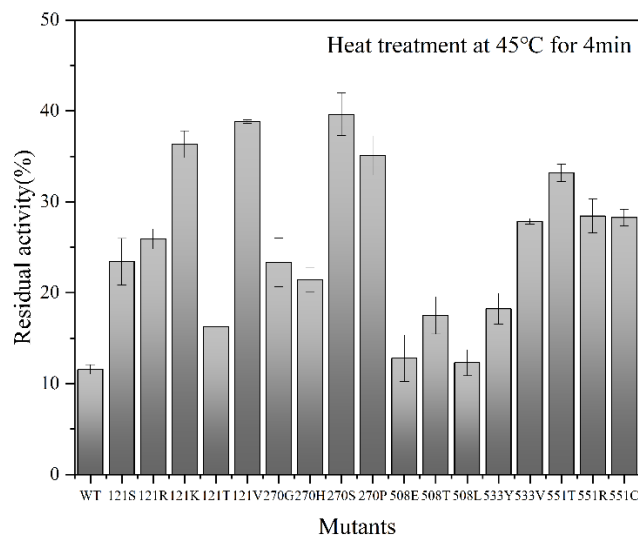


Figure 3. Positive mutants after high-throughput screening.

Table 1. Comparison of wild-type and point saturation mutation screening for optimal mutants.

GshFSA	$T_{1/2}$ at 40 °C (min)	Special Enzyme Activity (U/mg)
Wild type	5.69	1.47
R270S	14.88	1.53

2.3. Calculation of Un/Folding Free Energy and Modification of Single Variants

Structure-based and un/folding free energy calculations have also become widely used strategies in recent years, the most common selections for which were FoldX and Rosetta_ddg. The calculation of the un/folding free energy uses the energy function to describe the energy difference between the wild type and the mutants, which includes hydrogen bonding energy, van der Waals contributions, differences in solvation energy, etc. Additionally, Fireprot software can perform the free energy calculation of FoldX and Rosetta_ddg at the same time [20]. Firstly, we used the stable conformation after simulating 100 ns as a template for the next free energy calculation; secondly, FoldX was used to perform the calculation and screened out the potential mutants with $\Delta\Delta G < -1$ kcal/mol. Then, these mutants were passed through Rosetta_ddg for a free energy calculation to get the final recommended mutants. In the un/folding free energy calculation: $\Delta\Delta G = \Delta G_{\text{mutant}} - \Delta G_{\text{wildtype}}$. When $\Delta\Delta G$ is negative and the absolute value of this value is larger, it proves that the contribution of this mutation is higher [21]. The results of the calculations were as follows. All mutants were fermented in a shake flask, expressed and tested for half-life.

According to the results in Table 2, one mutant, N444W, had a mutation-decreased half-life, and the rest of the mutants were higher than the wild type. Among these mutants, three mutants had at least twice the half-life of the wild type, and the remaining six mutants had elevated but not significant half-lives. The best of them was mutant Q406M, which had a half-life of 18.21 min, 3.02 times higher than that of the wild type. In Figure 4, we plotted the thermal inactivation curves of all mutants with more than a twofold increase in half-value period. The above results indicated that this calculation of un/folding free energy could help to find some advantageous mutants quickly. However, to find the mutants with

great enhancement, further combinations of dominant sites or saturation mutations in these point mutations are needed to find amino acids that contribute more to stability.

Table 2. Results of un/folding free energy calculation and half-life of mutants.

Mutants	FoldX- $\Delta\Delta G$ (kcal/mol)	Rosetta_ddg- $\Delta\Delta G$ (kcal/mol)	$t_{1/2}$ at 40 °C (min)
S179M	−3.88	−2.9	15.18
S365P	−2.87	−4.61	11.69
I71W	−2.62	−10.81	7.74
S266M	−2.51	−6.55	6.67
N210G	−2.01	−9.11	6.47
Q206W	−1.94	−7.33	8.17
N444W	−1.91	−7.85	4.66
Q406M	−1.82	−8.72	18.21
L434F	−1.81	−5.44	6.69
A199F	−1.74	−9.43	6.13

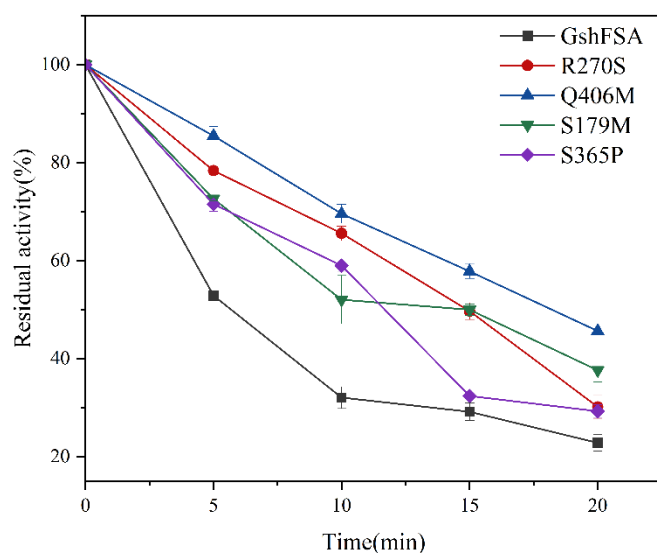


Figure 4. Thermal deactivation at 40°C of wild type and mutants.

2.4. Mechanistic Analysis

In order to explain the elevated thermal stability after mutation, we re-modeled the mutant with Alphafold2 and performed 50 ns molecular dynamics simulations at 298 K and 313 K using Gromacs. Based on Figure 5A, the simulation results of wild-type, R270S and Q406M mutants showed that the values of RMSD fluctuated stably in the range of 0.22–0.24 nm, which indicated that the simulation results were reliable.

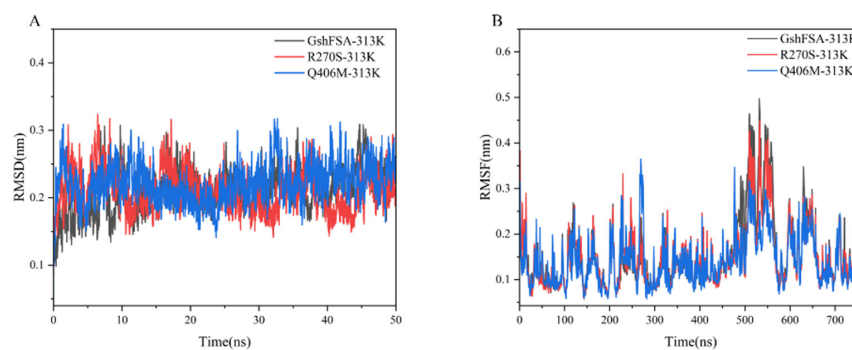


Figure 5. RMSD and RMSF values of WT, R270S and Q406M at 313 K. (A) RMSD values of GshFSA-313 K, R270S-313 K and Q406M-313 K; (B) RMSF values of GshFSA-313K, R270S-313 K and Q406M-313 K.

From Figure 5B, it could be found that the RMSF of wild type in the 510–570 region fluctuates more, which proved that this segment was more flexible. After mutation, the overall RMSF values of 510–570 region decreased. In particular, in Q406M, the RMSF values in this region decreased significantly, which indicated that mutation helped to stabilize the 510–570 region and increased the rigidity of this region. In the 270 site, the RMSF value of R270S is lower than that of wild type. These were the reasons for the increased stability after the mutation [22]. We could find that there was no significant change in RMSF at the 406 site before and after the mutation. It affected the stability by affecting the surrounding area. This also showed that the strategy of using molecular dynamics simulations to find high B-factor sites for saturation mutations was inherently limited, because it could not find key sites, like 406, that increase the surrounding region rather than increasing its own rigidity.

We superimposed WT-298 K, WT-313 K, R270S-298 K, R270S-313 K conformation using Pymol and calculated the average RMSD. The larger RMSD indicates the more unstable conformation. We found that the RMSD of WT was 1.691 in Figure 6A and that of R270S was 1.306 in Figure 6B. This indicated that the structure of a wild type collapsed significantly after the molecular dynamics simulation at a high temperature, while the conformation of R270S was more stable. In addition, as shown in Figure 6A, some loop regions in the conformation of the wild type were less superimposed, and the same loop regions was significantly better stacked in R270S, according to Figure 6B.

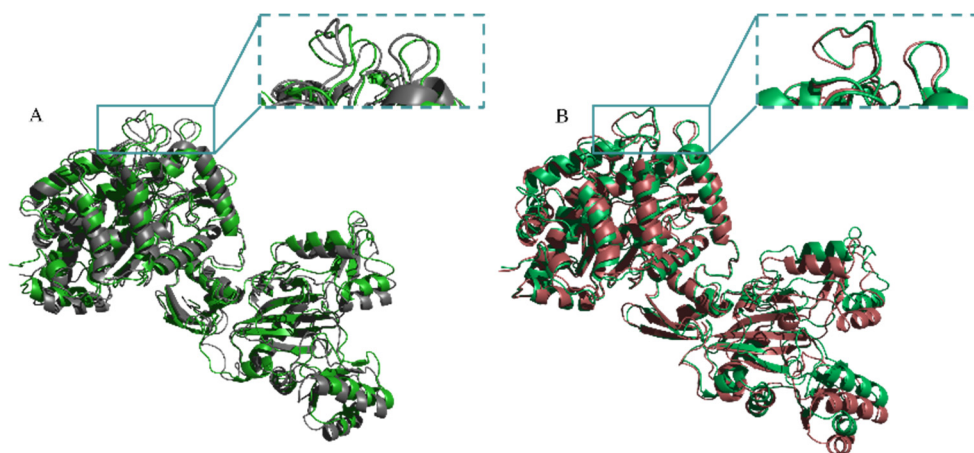


Figure 6. The structure superposition of WT and R270S. (A) The structure superposition of WT at 298 K and WT at 313 K; (B) The structure superposition of R270S at 298 K and R270S at 313 K.

After that, we performed hydrogen bonding analysis before and after mutation at site 270 by Pymol. The structures in the figure were all stable conformations after molecular dynamics simulations. As shown in Figure 7A, the wild type had one hydrogen bond between ARG270 and GLU243. Conversely, after mutation, Ser270 produced two stable hydrogen bonds with ASN271 and LEU273, as shown in Figure 7B. This indicated that one more hydrogen bond was produced after mutation. Additionally, hydrogen bond was also a significant factor in maintaining the protein structure and stability, and so this explained why the thermal stability of R270S was enhanced.

We superimposed WT-298 K, WT-313 K, Q406M-298 K, Q406M-313 K conformation using Pymol and calculated the average RMSD. We found that the RMSD of Q406M was 1.279 in Figure 8B. The RMSD was similarly lower than that of the wild type in Figure 8A, which also indicated that the mutant had better resistance to high temperature and was more stable. Additionally, according to the observations, some of the helix and loop regions of the wild type severely collapsed, with low degree of stacking and poor stability, while Q406M had a somewhat higher degree of stacking in the same regions.

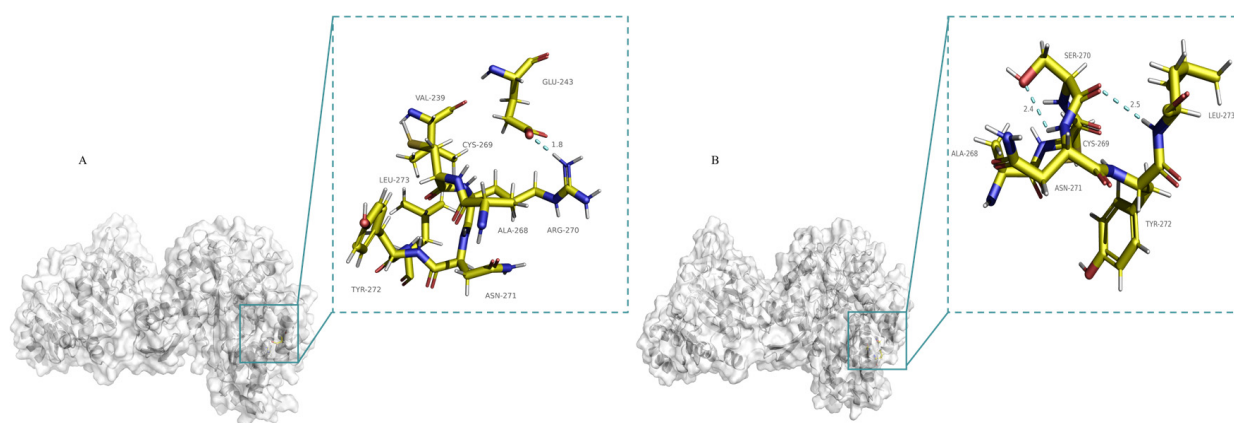


Figure 7. The hydrogen bond analysis. (A) The hydrogen bond analysis of WT; (B) The hydrogen bond analysis of R270S.

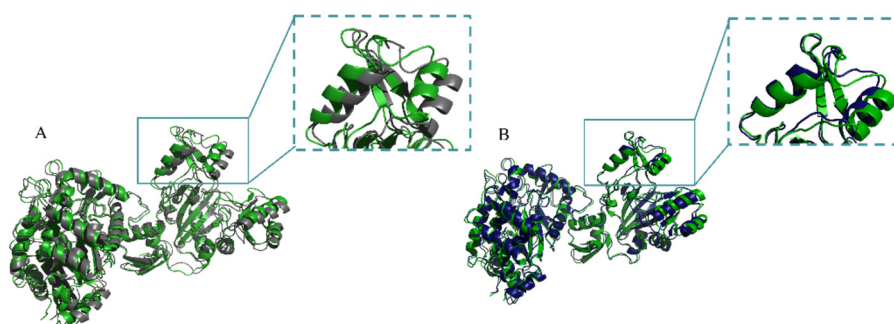


Figure 8. The structure superposition of WT and Q406M. (A) The structure superposition of WT at 298 K and WT at 313 K; (B) The structure superposition of Q406M at 298 K and Q406M at 313 K.

Above, we employed two strategies, the B-factor strategy and un/folding free energy calculation, to enhance the thermal stability of GshFSA. Both approaches have found their respective advantageous mutants, and the thermal stability of GshFSA has been improved. The mechanism could be explained from MD simulations, hydrogen bonding analysis, and conformational superposition. We found that each approach had its own limitations when used alone. Finding high B-factor sites to go through saturation mutations to reduce flexibility has been widely adopted. However, we should consider protein as a whole, sometimes as a dominant mutation, which is not a high flexibility site itself, but which enhances the rigidity of a region through synergy with nearby residues rather than the enhancement of its own rigidity. The calculation of un/folding free energy always had this problem of low accuracy and a large number of attempts are always needed, and scientists have already used graphical neural networks and Bayesian networks to predict the free energy efficiently and accurately [23]. Therefore, a simultaneous approach of both strategies can be adopted to find dominant mutants more widely and quickly while avoiding the need to conduct large-scale random mutation screening. In the thermal stability modification of keratinase, Su et al. used a molecular dynamic simulation strategy to identify 22 flexible sites based on the B-factor, and each site was virtually screened based on un/folding free energy calculation to streamline the experiment and improve the screening accuracy [24]. This simultaneous use of multiple methods can greatly improve the screening efficiency and accurately find the key sites affecting the thermal stability.

3. Materials and Methods

3.1. Strains and Culture Medium

E. coli BL21 (DE3) was used for enzyme expression, and *E. coli* Top10 was used for plasmid propagation. All of the strains were purchased from Shanghai Weidi Biotechnology

Co., Ltd. (Shanghai, China). The enzymes and mutants were all expressed in Luria Bertani (LB) medium (tryptone 10 g/L, yeast extract 5 g/L, NaCl 10 g/L, 50 ug/mL kanamycin). The induction temperature was 30 °C and 0.2 mM of isopropyl- β -D, thiogalactopyranoside (IPTG) was added for overexpression. The tryptone and yeast extract were purchased from Oxoid (UK), other reagents in Section 3.1 were purchased from Sigma (Shanghai, China).

3.2. Construction of Mutants

The strategy for point-saturated library construction was the NNK, by designing primers, adding equal proportions of bases at the mutation site. We achieved mutant library construction with Mut Express II Fast Mutagenesis Kit V2 supplied by Vazyme (Nanjing, China). PCR was performed for 30 cycles consisting of 30 s at 95 °C, 15 s at 95 °C, 15 s at 60 °C, 6 min at 72 °C, 5 min at 72 °C. The method for point mutations was constructed as above.

3.3. Enzyme Activity and Thermal Stability Assay

The enzymatic activity of GshFSA was assayed as follows. There was a reaction system of 1 mL: the substrates were 40 mM glycine, 20 mM cysteine, 40 mM glutamate, 20 mM ATP and 20 mM MgCl₂. The reaction was carried out in 200 mM Tris-HCl (pH 8.5) for 10 min, and the reaction was terminated with 20% (*v/v*) trichloroacetic acid, and the activity assay was performed using the specific reaction of tetraoxypyrimidine with glutathione, which concluded with 700 μ L 200 mM PBS, 100 μ L 7.5 g/L glycine, 100 μ L 1 g/L tetraoxypyrimidine, and 100 μ L reaction solution. After a 20 min reaction at 30 °C, the standard curve was plotted and the enzyme activity was calculated by Abs 305 nm. All of these reagents in Section 3.3 were purchased from Shanghai yuan ye Bio-Technology Co. Ltd. (Shanghai, China).

We used $t_{1/2}$ as a parameter to evaluate the thermal stability of the enzyme. $T_{1/2}$ is the kinetic parameter of the enzyme and refers to the time required for the enzyme activity to drop to half of the initial one. We placed the wild type and mutants in a metal bath at 40 °C and kept taking samples over time to test the remaining enzyme activity and plot the thermal inactivation curve.

3.4. High Throughput Screening

After constructing the mutant library, we performed the following steps for the culture and screening of the mutant library: single colonies from the plates were picked into 96 deep-well plates as the primary culture and incubated at 37 °C and 900 rpm for 8 h. Then, we inoculated primary culture into the secondary deep-well plate at 1% inoculum and incubated it for 3 h; we then added 0.2 mM IPTG and incubated for 12 h at 30 °C and 700 rpm.

Then, we set the centrifuge parameters to 3000 \times g rpm, 5 min, and 4 °C to collect the bacteria. We added Tris-HCl (pH 8.5) for resuspension, a freeze–thaw experiment was performed three times to complete cell fragmentation, and we centrifuged again to collect the crude enzyme solution.

We completed the enzyme activity assay in a 96-well plate, the enzyme activity assay was shown in Section 3.3. All mutants were directly placed in heat treatment at 45 °C for 4 min and the remaining enzyme activity assay was performed. After heat treatment, the spots with high residual activity were selected for sequencing validation and shake flask re-screening.

3.5. Model Construction and Molecular Dynamics Simulation

In this study, both wild type and mutant models were constructed by AlphaFold2 which was developed by Deepmind from UK (colab.research.google.com/github/sokrypton/ColabFold/blob/main/AlphaFold2.ipynb, accessed on 27 October 2021), and all molecular dynamics simulation procedures were performed by Gromacs (Groningen, The Nether-

lands, Version 2021.4). The structure presentation and comparative analysis were all performed by Pymol (USA, Version 2.5.4).

3.6. Un/Folding Energy Calculation

In this study, we used Fireprot (loschmidt.chemi.muni.cz/fireprotweb, accessed on 25 March 2022) to perform the calculation of un/folding free energy, uploaded the protein conformation after molecular dynamics simulation to the Fireprot (Czechia), observed the Gibbs free energy calculation results of FoldX and Rosetta in its energy mutant module, and sorted and selected the modification sites.

4. Conclusions

In this article, the B-factor strategy and un/folding free energy calculation strategy were both used to enhance the thermal stability of GshFSA. Molecular dynamics simulations were performed by Gromacs to calculate the B-factor of each residue. Five highly flexible sites were investigated and site-saturation mutations were performed. A total of 17 positive mutants were finally identified by high-throughput screening, the best of which was R270S with a 2.62-fold increase in half-life compared to the wild type; meanwhile, 10 mutants were also predicted and validated by performing un/folding free energy calculations based on the structure. Of those identified, 3 mutants were found to be more than twofold higher than the wild type, and the best one was Q406M, which was 3.02-fold higher than the wild type with a half-life of 18.21 min. The mechanism of thermal stability enhancement was studied from the perspectives of molecular dynamics simulation, conformational comparison, and hydrogen bonding analysis. However, the B-factor showed some limitations: it is not possible to discover low B-factor site that influences the nearby regions and thus enhance the overall rigidity, and the un/folding free energy calculation strategy also has some accuracy problems. This strategy could combine the advantages of B-factor and free energy calculation to find the superior mutants simultaneously from multiple angles, which can achieve more rapid and accurate enhancement of enzyme thermal stability. In the future, there is strong necessity to carry out the combination of multiple dominant mutants, which may find dominant stacked combinatorial mutants to further enhance the thermal stability of GshFSA.

Author Contributions: W.Z. and H.S. performed the experiments. Q.J. and R.Z. assisted with the simulation calculations. Q.W. and Q.Z. assisted with data analysis. L.L. and H.C. designed the experiment. All authors have read and agreed to the published version of the manuscript.

Funding: This work was supported by the National Key Research and Development Program of China (grant number 2021YFF0600703).

Data Availability Statement: Not applicable.

Conflicts of Interest: The authors declare no conflict of interest.

References

1. Wang, Y.; Liu, Y.; Ding, F.; Zhu, X.; Yang, L.; Zou, P.; Rao, H.; Zhao, Q.; Wang, X. Colorimetric determination of glutathione in human serum and cell lines by exploiting the peroxidase-like activity of CuS-polydopamine-Au composite. *Anal. Bioanal. Chem.* **2018**, *410*, 4805–4813. [[CrossRef](#)] [[PubMed](#)]
2. Patzschke, A.; Steiger, M.G.; Holz, C.; Lang, C.; Mattanovich, D.; Sauer, M. Enhanced glutathione production by evolutionary engineering of *Saccharomyces cerevisiae* strains. *Biotechnol. J.* **2015**, *10*, 1719–1726. [[CrossRef](#)] [[PubMed](#)]
3. Li, Y.; Wei, G.; Chen, J. Glutathione: A review on biotechnological production. *Appl. Microbiol. Biotechnol.* **2004**, *66*, 233–242. [[CrossRef](#)] [[PubMed](#)]
4. Wang, C.; Zhang, J.; Wu, H.; Li, Z.; Ye, Q. Heterologous gshF gene expression in various vector systems in *Escherichia coli* for enhanced glutathione production. *J. Biotechnol.* **2015**, *214*, 63–68. [[CrossRef](#)]
5. Zhang, X.; Wu, H.; Huang, B.; Li, Z.; Ye, Q. One-pot synthesis of glutathione by a two-enzyme cascade using a thermophilic ATP regeneration system. *J. Biotechnol.* **2017**, *241*, 163–169. [[CrossRef](#)] [[PubMed](#)]
6. Janowiak, B.E.; Griffith, O.W. Glutathione synthesis in *Streptococcus agalactiae*: One protein accounts for γ -glutamylcysteine synthetase and glutathione synthetase activities. *J. Biol. Chem.* **2005**, *280*, 11829–11839. [[CrossRef](#)] [[PubMed](#)]

7. Traxlmayr, M.W.; Obinger, C. Directed evolution of proteins for increased stability and expression using yeast display. *Arch. Biochem. Biophys.* **2012**, *526*, 174–180. [[CrossRef](#)] [[PubMed](#)]
8. Tompa, D.R.; Gromiha, M.M.; Saraboji, K. Contribution of main chain and side chain atoms and their locations to the stability of thermophilic proteins. *J. Mol. Graph. Model.* **2016**, *64*, 85–93. [[CrossRef](#)] [[PubMed](#)]
9. Kim, Y.E.; Hipp, M.S.; Bracher, A.; Hayer-Hartl, M.; Ulrich Hartl, F. Molecular chaperone functions in protein folding and proteostasis. *Annu. Rev. Biochem.* **2013**, *82*, 323–355. [[CrossRef](#)]
10. Sanchez-Ruiz, J.M. Protein kinetic stability. *Biophys. Chem.* **2010**, *148*, 1–15. [[CrossRef](#)]
11. Blum, J.K.; Ricketts, M.D.; Bommaris, A.S. Improved thermostability of AEH by combining B-FIT analysis and structure-guided consensus method. *J. Biotechnol.* **2012**, *160*, 214–221. [[CrossRef](#)] [[PubMed](#)]
12. Delgado, J.; Radusky, L.G.; Cianferoni, D.; Serrano, L. FoldX 5.0: Working with RNA, small molecules and a new graphical interface. *Bioinformatics* **2019**, *35*, 4168–4169. [[CrossRef](#)] [[PubMed](#)]
13. Xing, H.; Zou, G.; Liu, C.; Chai, S.; Yan, X.; Li, X.; Liu, R.; Yang, Y.; Zhou, Z. Improving the thermostability of a GH11 xylanase by directed evolution and rational design guided by B-factor analysis. *Enzym. Microb. Technol.* **2021**, *143*, 109720. [[CrossRef](#)]
14. Bell, E.L.; Smithson, R.; Kilbride, S.; Foster, J.; Hardy, F.J.; Ramachandran, S.; Tedstone, A.A.; Haigh, S.J.; Garforth, A.A.; Day, P.J. Directed evolution of an efficient and thermostable PET depolymerase. *Nat. Catal.* **2022**, *5*, 673–681. [[CrossRef](#)]
15. Zhang, X.; Li, W.; Pan, L.; Yang, L.; Li, H.; Ji, F.; Zhang, Y.; Tang, H.; Yang, D. Improving the thermostability of alginate lyase FLAlyA with high expression by computer-aided rational design for industrial preparation of alginate oligosaccharides. *Front. Bioeng. Biotechnol.* **2022**, *10*, 1011273. [[CrossRef](#)] [[PubMed](#)]
16. Romero, P.A.; Krause, A.; Arnold, F.H. Navigating the protein fitness landscape with Gaussian processes. *Proc. Natl. Acad. Sci. USA* **2013**, *110*, E193–E201. [[CrossRef](#)]
17. Jumper, J.; Evans, R.; Pritzel, A.; Green, T.; Figurnov, M.; Ronneberger, O.; Tunyasuvunakool, K.; Bates, R.; Žídek, A.; Potapenko, A. Highly accurate protein structure prediction with AlphaFold. *Nature* **2021**, *596*, 583–589. [[CrossRef](#)]
18. Garg, P.; Vanamamalai, V.K.; Jali, I.; Sharma, S. In silico prediction of the animal susceptibility and virtual screening of natural compounds against SARS-CoV-2: Molecular dynamics simulation based analysis. *Front. Genet.* **2022**, *13*, 906955. [[CrossRef](#)]
19. Lu, T.; Tan, H.; Lee, D.; Chen, G.; Jia, Z. New insights into the activation of Escherichia coli tyrosine kinase revealed by molecular dynamics simulation and biochemical analysis. *Biochemistry* **2009**, *48*, 7986–7995. [[CrossRef](#)]
20. Musil, M.; Stourac, J.; Bendl, J.; Brezovsky, J.; Prokop, Z.; Zendulka, J.; Martinek, T.; Bednar, D.; Damborsky, J. FireProt: Web server for automated design of thermostable proteins. *Nucleic Acids Res.* **2017**, *45*, W393–W399. [[CrossRef](#)]
21. Bednar, D.; Beerens, K.; Sebestova, E.; Bendl, J.; Khare, S.; Chaloupkova, R.; Prokop, Z.; Brezovsky, J.; Baker, D.; Damborsky, J. FireProt: Energy-and evolution-based computational design of thermostable multiple-point mutants. *PLoS Comput. Biol.* **2015**, *11*, e1004556. [[CrossRef](#)] [[PubMed](#)]
22. Bi, J.; Chen, S.; Zhao, X.; Nie, Y.; Xu, Y. Computation-aided engineering of starch-debranching pullulanase from Bacillus thermoleovorans for enhanced thermostability. *Appl. Microbiol. Biotechnol.* **2020**, *104*, 7551–7562. [[CrossRef](#)] [[PubMed](#)]
23. Wang, S.; Tang, H.; Zhao, Y.; Zuo, L. BayeStab: Predicting effects of mutations on protein stability with uncertainty quantification. *Protein Sci.* **2022**, *31*, e4467. [[CrossRef](#)] [[PubMed](#)]
24. Su, C.; Gong, J.-S.; Qin, A.; Li, H.; Li, H.; Qin, J.; Qian, J.-Y.; Xu, Z.-H.; Shi, J.-S. A combination of bioinformatics analysis and rational design strategies to enhance keratinase thermostability for efficient biodegradation of feathers. *Sci. Total Environ.* **2022**, *818*, 151824. [[CrossRef](#)] [[PubMed](#)]